J|A|C|S ARTICLES

Published on Web 08/12/2009

Synthesis and Characterization of Nucleobase−Carbon Nanotube Hybrids

Prabhpreet Singh,[†] Jitendra Kumar,[‡] Francesca Maria Toma,[§,||] Jesus Raya,[⊥] Maurizio Prato,[§] Bruno Fabre,[#] Sandeep Verma,*[,‡] and Alberto Bianco*[,†]

CNRS, Institut de Biologie Moléculaire et Cellulaire, Laboratoire d'Immunologie et Chimie Thérapeutiques, 67000 Strasbourg, France, Department of Chemistry, Indian Institute of Technology, Kanpur-208016 UP, India, Dipartimento di Scienze Farmaceutiche, Università di Trieste, 34127 Trieste, Italy, SISSA, Via Beirut 2−4, 34151 Trieste, Italy, Laboratoire de RMN et de biophysique des membranes, Institut de Chimie, UMR 7177 CNRS, Université de Strasbourg, 67000 Strasbourg, France, Matière Condensée et Systèmes Electroactifs MaCSE, UMR 6226 Sciences Chimiques de Rennes, CNRS/Université de Rennes 1, Campus de Beaulieu, 35042 Rennes, France

Received June 24, 2009; E-mail: sverma@iitk.ac.in; a.bianco@ibmc.u-strasbg.fr

Abstract: We report the synthesis and characterization of adenine−single-walled carbon nanotube (SWCNT) hybrid materials, where for the first time nucleobases are covalently attached to the exosurface of SWCNTs. The structural properties of all hybrids have been characterized using usual spectroscopic and microscopic techniques. The degree of functional groups for functionalized SWCNTs (*f*-SWCNTs) **2a** and **2b** is one adenine group for each 26 and 37 carbon atoms, respectively. Solid-state magic angle spinning ^{13}C NMR spectroscopy (MAS NMR) and electrochemistry have been also applied for the characterization of these *f*-SWCNTs. AFM images of *f*-SWCNT **2b** showed an interesting feature of horizontally aligned nanotubes along the surface when deposited on highly oriented pyrolytic graphite surface. Furthermore, we evaluated the coordinating ability of these hybrid materials toward silver ions, and interestingly, we found a pattern of silver nanoparticles localized over the surface of the carbon nanotube network. The presence of aligned and randomly oriented CNTs and their ability to coordinate with metal ions make this class of materials very interesting for applications in the development of novel electronic devices and as new supports for different catalytic transformations.

Introduction

Carbon nanotubes (CNTs),[1−4] due to their unique one-dimensional nanostructure and remarkable mechanical, thermal, optical, and electronic properties,[5−8] may find many applications in both materials and life sciences.[7−10] Although CNTs possess very low solubility in aqueous as well as organic solvents, which has been a major barrier for a variety of potential uses, covalent functionalization of CNTs is a powerful way to improve both dispersion and interaction. In recent years, interest has focused on chemical functionalization of single-walled carbon nanotubes (SWCNTs), and in this regard, a wide variety of reactions have been developed, including oxidation at defect sites followed by amidation and esterification reactions, fluorination, addition of diazonium salts, and radicals and 1,3-dipolar cycloaddition reactions, to name a few.[11−15]

Nucleic acids can exist in different forms, and this diversity can be correlated with their different biological functions.[16,17] Nucleobases are the fundamental constituents of nucleic acids and provide hydrogen binding aided molecular recognition for the formation of duplexes, triplexes, tetraplexes, and higher order

[†] CNRS.
[‡] Indian Institute of Technology.
[§] Università di Trieste.
[||] SISSA.
[⊥] Université de Strasbourg.
[#] CNRS/Université de Rennes 1.

(1) Monthioux, M.; Kuznetsov, V. L. *Carbon* **2006**, *44*, 1621–1623.
(2) Iijima, S. *Nature* **1991**, *354*, 56–58.
(3) Iijima, S.; Ichihashi, T. *Nature* **1993**, *363*, 603–605.
(4) Bethune, D. S.; Klang, C. H.; de Vries, M. S. *Nature* **1993**, *363*, 605–607.
(5) Haddon, R. C., Guest Ed. Special issue on Carbon Nanotubes. *Acc. Chem. Res.* **2002**, *35*, 997−1113.
(6) Rao, C. N. R.; Satishkumar, B. C.; Govindaraj, A.; Nath, M. *ChemPhysChem* **2001**, *2*, 78–105.
(7) Jorio, A.; Dresselhaus, G.; Dresselhaus, M. S. *Carbon Nanotubes: Advanced Topics in the Synthesis, Structure, Properties and Applications*; Springer: Berlin, 2008.
(8) Reich, S.; Thomsen, C.; Maultzsch, J. *Carbon Nanotubes: Basic Concepts and Physical Properties*; Wiley-VCH: Germany, 2004.
(9) Kreupl, F. *Carbon Nanotubes in Microelectronic Applications*; Wiley-VCH: Germany, 2008.
(10) Cataldo, F.; Da Ros, T. *Medicinal Chemistry and Pharmacological Potential of Fullerenes and Carbon Nanotubes*; Springer: Berlin, 2008.
(11) Singh, P.; Campidelli, S.; Giordani, S.; Bonifazi, D.; Bianco, A.; Prato, M. *Chem. Soc. Rev.* **2009**, *38*, 2214–2230.
(12) Tasis, D.; Tagmatarchis, N.; Bianco, A.; Prato, M. *Chem. Rev.* **2006**, *106*, 1105–1136.
(13) Banerjee, S.; Hemraj-Benny, T.; Wong, S. S. *Adv. Mater.* **2005**, *17*, 17–29.
(14) Dyke, C. A.; Tour, J. M. *Chem.—Eur. J.* **2004**, *10*, 812–817.
(15) Hirsch, A. *Angew. Chem., Int. Ed.* **2002**, *41*, 1853–1859.
(16) Sinden, R. R. *DNA Structure and Function*; Academic Press: San Diego, CA, 1994.
(17) Neidle, S. *Oxford Handbook of Nucleic Acid Structure*; Oxford University Press: New York, 1999.

architectures.[18] Nucleic acids (DNA and RNA) have been explored to noncovalently functionalize CNTs toward various biomedical applications ranging from nanodevices, gene therapy, and drug delivery to membrane separation.[19−21]

Noncovalent interactions and the ability of nucleobases to disperse SWCNTs have been evaluated theoretically and experimentally.[22−27] It has been reported that poly(T) single-stranded DNA (ssDNA) could more efficiently disperse SWCNTs in water than poly(A) and poly(C), as confirmed later using density functional theory.[23,24] It was proposed that thymine possesses the lowest self-stacking tendency and a higher ability to disperse the SWCNTs via π-stacking. Recently, using the *ab initio* Hartree−Fock method together with classical force field, it was shown that experimental binding energies of nucleobases with SWCNTs in aqueous solution decrease in the order G > T > A > C.[25] It has also been reported that carboxyl- or hydroxyl-modified SWCNTs can facilitate the self-structuring of ssRNA poly(rA) to form an $A \cdot A^+$ duplex-like structure.[26] In addition, Hg(II) ions have a strong and specific binding affinity for the nucleic bases of ssDNA noncovalently wrapped around SWCNTs.[27]

However, nucleobases have not yet been used for covalent attachment on CNTs. We anticipate that discrete superstructures arising from nucleobase−CNT hybrids will likely reveal interesting structures and properties, including DNA recognition or self-assembly, on the sheer basis of base-pair complementarity. These heterocyclic molecules also have an ability to coordinate a variety of metal ions, which could be used for the stabilization of superstructures as well as to support metal-aided catalytic transformations. Therefore, new hybrid materials comprising both nucleobases and CNTs would be extremely interesting in view of the remarkable properties of CNTs and recognition properties of nucleobases.

In this work, we describe the synthesis and the characterization, using different analytical and microscopic techniques, including solid-state NMR and electrochemistry, of adenine−SWCNT hybrid materials prepared by amidation reactions between acid/amine-functionalized SWCNTs and amine/acid-functionalized adenine derivatives. The possibility to generate controlled horizontal alignment of the nanotubes on highly oriented pyrolytic graphite (HOPG) surfaces and the complexation with metal ions disclose unprecedented opportunities for highly patterned supramolecular assembly of SWCNTs. This will open the door to applications of these hybrids as novel CNT-based nanowires in nanoelectronics, biosensing, and catalysis.

Results and Discussion

Synthesis of the Nucleobase−Carbon Nanotube Hybrids. Purified and oxidized SWCNT-COOH **1a** was obtained after modification of earlier reported procedures involving reaction of pristine HiPco SWCNTs (Scheme 1).[28] The strong acid treatment generates defects on the side walls and forms open ends that are both terminated by carboxylic acid groups. The loading (amount of functional groups) was calculated after derivatization of the carboxylic groups (activated as acid chlorides) with Boc-monoprotected diaminotriethylene glycol. The Boc group was removed with HCl solution in dioxane to afford functionalized single-walled carbon nanotubes (*f*-SWCNTs) **1b**. The number of free amino groups was measured with a quantitative Kaiser test. Nucleobases were modified with reactive functionalities for conjugation with CNTs. We prepared the 3-(9-adeninyl)propionic acid ethyl ester, which was eventually deprotected to obtain the corresponding 3-(9-adeninyl)propionic acid **4** in good yields. Alternatively, we prepared adenine derivative 9-(2-aminoethyl)adenine **3**, containing an amino group. *f*-SWCNT **2a** was synthesized following the acyl chloride route, allowing the SWCNT-COOH **1a** to react with oxalyl chloride under argon at refluxing conditions. The resulting acid chloride derivative, SWCNT-COCl, was then heated under reflux with adenine derivative **3** to afford adenine-functionalized *f*-SWCNT **2a**. 3-(9-Adeninyl)propionic acid **4** was activated using standard coupling reagents and then condensed with *f*-SWCNT **1b** to afford *f*-SWCNT **2b**.

Characterization of the Nucleobase−Carbon Nanotube Hybrids. The degree of functionalization for the oxidized SWCNT-COOH **1a** and the functionalized conjugates (*f*-SWCNTs **1b**, **2a**, and **2b**) has been evaluated by thermogravimetric analysis (TGA) under N_2 atmosphere (Figure 1). The TGA curves of *f*-SWCNT **2a** and *f*-SWCNT **2b** show a gradual weight loss of about 39.6% and 45.9% at 600 °C, respectively, as compared to 22.0% of the oxidized SWCNT-COOH **1a** and 29.4% of the *f*-SWCNT **1b**, respectively. On the basis of weight loss, we estimated that the degree of functionalization for *f*-SWCNT **2a** and **2b** is of one adenine group each, 26 and 37 carbon atoms, respectively.

The infrared spectra (as KBr pellets) of SWCNT-COOH **1a** and *f*-SWCNTs **1b**, **2a**, and **2b** also confirmed covalent functionalization because of the structural modifications that occurred. The FT-IR spectrum of SWCNT-COOH **1a** shows four broad absorption peaks at 1399, 1594, 1732, and 3421 cm^{-1}, corresponding to the carboxylic groups' vibrational motions, like C−O−H bending, asymmetric stretching corresponding to carboxylate anion (COO^-), C=O symmetric stretching, and the U-shaped O−H stretching respectively (Figure 2, top). For *f*-SWCNT **2a**, an absorption peak at 1594 cm^{-1}, with a shoulder at 1645 cm^{-1}, and one at 1730 cm^{-1}, similar in shape and frequency to that found at 1732 cm^{-1} in the spectrum of **1a**, due to the incomplete conversion of carboxylic groups, were clearly observed. These peaks are assigned to the N−H bending of CONH, the C=O stretching of CONH, and the C=O stretching of COOH, respectively. Some broad absorption bands centered at 3437 cm^{-1} with a

(18) Suhnel, J. *Biopolymers* **2002**, *61*, 32–51.
(19) Bianco, A.; Kostarelos, K.; Partidos, C. D.; Prato, M. *Chem. Commun.* **2005**, *5*, 571–577.
(20) Lacerda, L.; Bianco, A.; Prato, M.; Kostarelos, K. *J. Mater. Chem.* **2008**, *18*, 17–22.
(21) Lu, F.; Gu, L.; Meziani, M. J.; Wang, X.; Luo, P. G.; Veca, L. M.; Cao, L.; Sun, Y.-P. *Adv. Mater.* **2009**, *21*, 139–152.
(22) Gowtham, S.; Scheicher, R. H.; Pandey, R.; Karna, S. P.; Ahuja, R. *Nanotechnology* **2008**, *19*, 125701.
(23) Zheng, M.; Jagota, A.; Semke, E. D.; Diner, B. A.; Mclean, R. S.; Lustig, S. R.; Richardson, R. E.; Tassi, N. G. *Nat. Mater.* **2003**, *2*, 338–342.
(24) Wang, Y. *J. Phys. Chem. C* **2008**, *112*, 14297–14305.
(25) Varghese, N.; Mogera, U.; Govindaraj, A.; Das, A.; Maiti, P. K.; Sood, A. K.; Rao, C. N. R. *ChemPhysChem* **2009**, *10*, 206–210.
(26) Zhao, C.; Peng, Y.; Song, Y.; Ren, J.; Qu, X. *Small* **2008**, *4*, 656–661.
(27) Gao, X.; Xing, G.; Yang, Y.; Shi, X.; Liu, R.; Chu, W.; Jing, L.; Zhao, F.; Ye, C.; Yuan, H.; Fang, X.; Wang, C.; Zhao, Y. *J. Am. Chem. Soc.* **2008**, *130*, 9190–9191.
(28) Kam, N. W. S.; Jessop, T. C.; Wender, P. A.; Dai, H. *J. Am. Chem. Soc.* **2004**, *126*, 6850–6851.

Scheme 1. Synthesis of SWCNT Derivatives **1a** and **1b** and Adenine−CNT Hybrids **2a** and **2b**

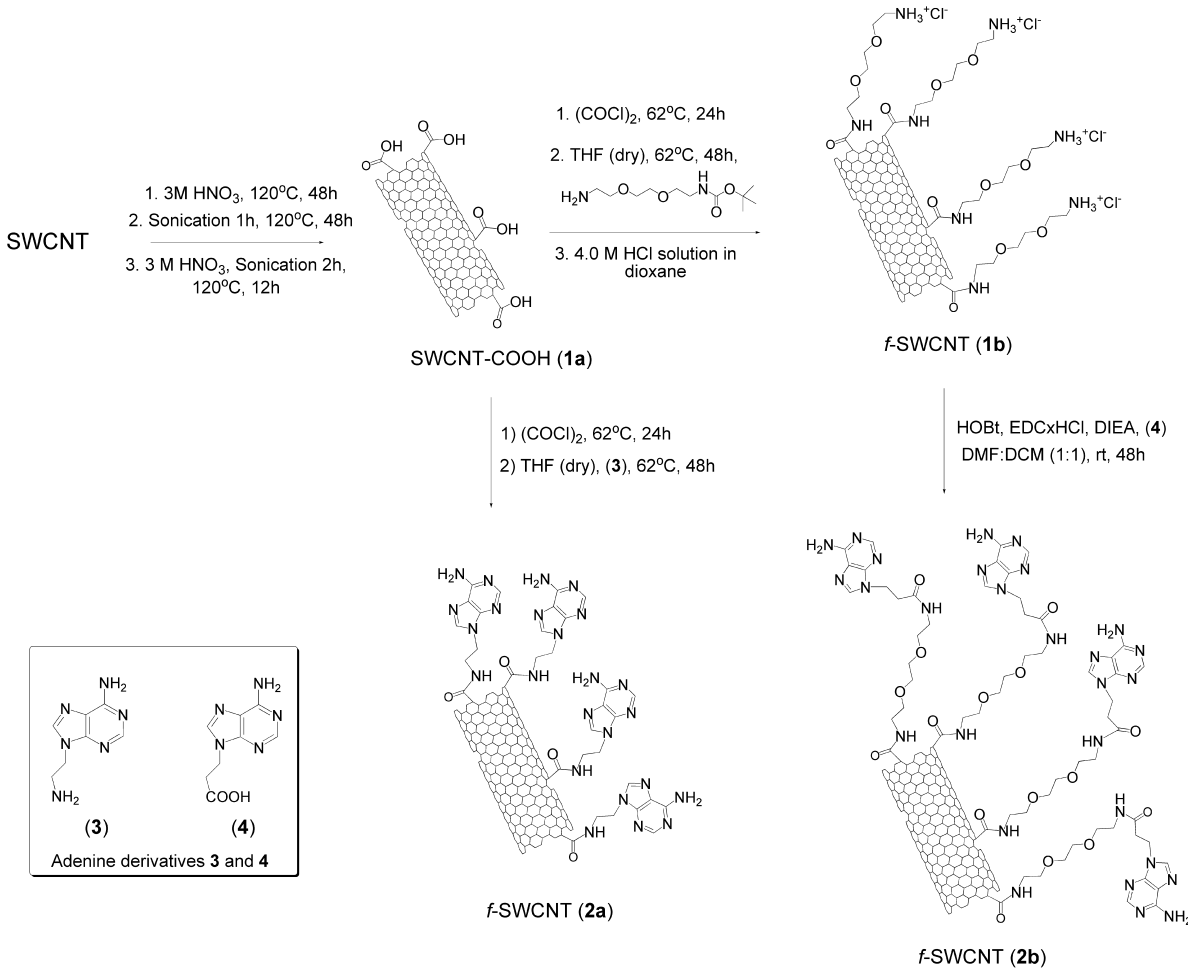

shoulder at 3390 cm^{-1} in the spectrum of *f*-SWCNT **2a** were visible. These signals are not present in the SWCNT-COOH **1a** spectrum, proving the conversion of most of the COOH into the amide groups of **2a**.

The FT-IR spectrum of Boc-protected *f*-SWCNT **1b** and Boc-deprotected *f*-SWCNT **1b** shows absorption peaks around 1586 and 1593 cm^{-1} corresponding to the N−H bending of CONH; a shoulder peak at 1626 and 1650 cm^{-1} corresponds to the C═O stretching of CONH, respectively. The absorption at 1735 cm^{-1} is similar to that at 1732 cm^{-1} found in the SWCNT-COOH **1a**. Comparison of the two spectra indicates that absorption peaks at 1519 and 1699 cm^{-1} and a small absorption peak at 2971 cm^{-1} are present only in the Boc-protected nanotubes (Figure 2, bottom). These signals are not present in the Boc-deprotected *f*-SWCNT **1b** spectrum, so these absorption peaks are assigned to the N−H bending of carbamates, C═O stretching of carbamates, and $-CH_3$ asymmetric stretching of the *tert*-butyl group, respectively. Finally, in the FT-IR spectrum of *f*-SWCNT **2b**, a very strong and broad absorption peak at 1595 cm^{-1} corresponding to N−H bending of CONH, and one at 1737 cm^{-1} due to incomplete conversion of the carboxylic group (as confirmed by the Kaiser test), were observed (Figure 2, bottom). In all spectra, two weak signals around 2860 and 2920 cm^{-1} were detected and were assigned to symmetric and asymmetric $-CH_2-$ stretching due to the diaminotriethylene glycol linker.

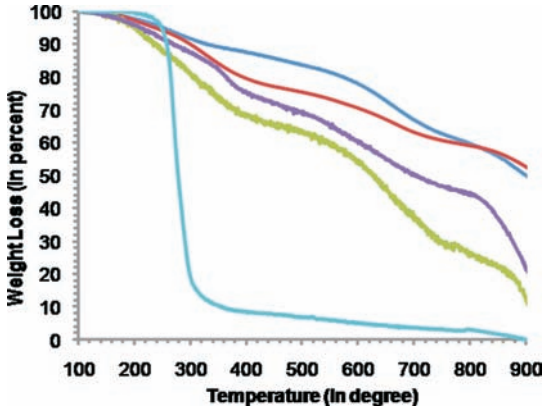

Figure 1. Thermogravimetric analysis for SWCNT-COOH **1a** (blue), *f*-SWCNT **1b** (red), *f*-SWCNT **2a** (magenta), *f*-SWCNT **2b** (green), and adenine acid **4** (cyan) in N_2 atmosphere with a ramp of 10 °C/min.

NMR spectroscopy is not routinely used to characterize functionalized CNTs.[29] Indeed, proton analysis in solution gives very weak and broad signals, and most of the NMR studies have been performed using solid-state analysis.[30−32] We have decided to carry out solid-state ^{13}C NMR spectroscopy using magic angle spinning (MAS). Synchronized Hahn-echo and $^{1}H-^{13}C$ cross-polarization (CP) pulse sequences were applied

(29) Marega, R.; Aroulmoji, V.; Dinon, F.; Vaccari, L.; Giordani, S.; Bianco, A.; Murano, E.; Prato, M. *J. Am. Chem. Soc.* **2009**, *131*, 9086–9093.

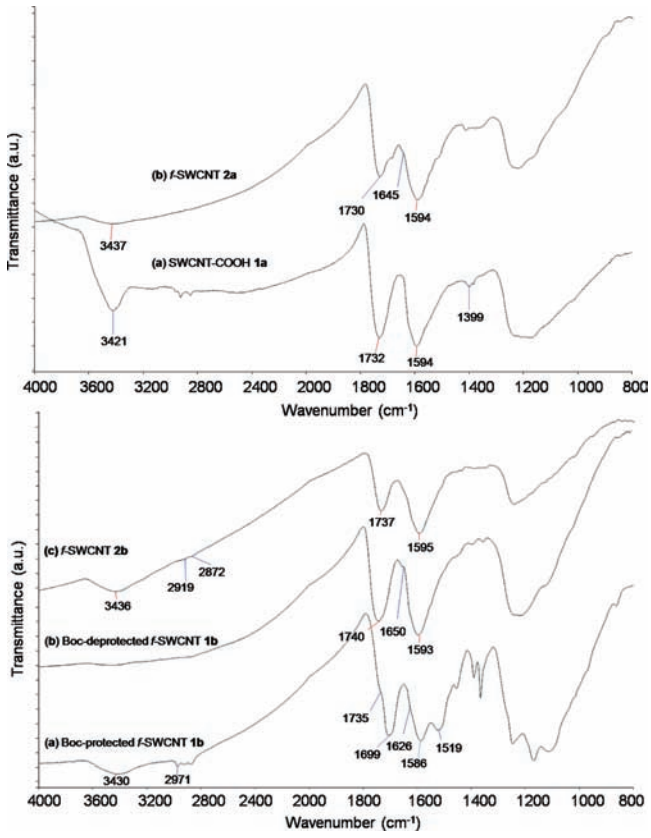

Figure 2. Infrared spectra of (top) SWCNT-COOH (a) and *f*-SWCNT **2a** (b), and (bottom) Boc-protected *f*-SWCNT **1b** (a), Boc-deprotected *f*-SWCNT **1b** (b), and *f*-SWCNT **2b** (c). The principal absorption features are highlighted with the correspondent wavenumbers.

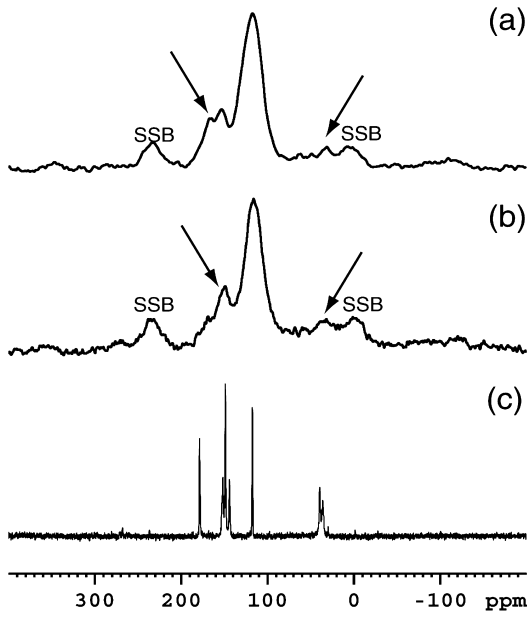

Figure 3. MAS ^{13}C NMR Hahn-echo spectra of (a) SWCNT-COOH **1a**, (b) *f*-SWCNT **2a**, and (c) adenine base alone. SSB indicates spinning sidebands from the rotor's Kel-F cap used for NMR. The regions indicated by arrows highlight the major changes in the spectra.

to the samples for the characterization of SWCNTs and their derivatives. Figure 3a shows a very strong ^{13}C NMR resonance around 117 ppm for the SWCNT-COOH **1a** sample, along with other resonances at 151 and 166 ppm corresponding to aromatic

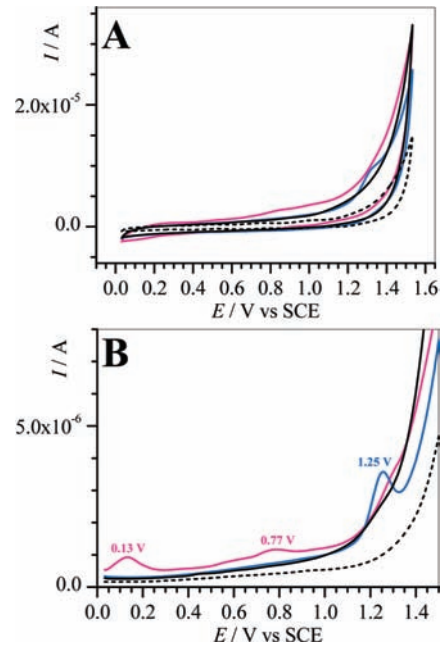

Figure 4. (A) CV at 0.1 V s^{-1} and (B) corresponding DPV responses of *f*-SWCNT **2a** (blue) and **2b** (magenta), SWNT-COOH **1a** (black, solid line), and electrolyte alone (black, dashed line). *f*-SWCNT conjugate concentration: 0.25 mg mL^{-1}.

and carbonyl carbons, respectively. The MAS ^{13}C NMR spectrum of *f*-SWCNT **2a** (Figure 3b) shows changes in the 25−42 and 150−170 ppm regions due to the presence of adenine signals and conversion of the acid group into an amide functionality. The peak at 166 ppm present in the SWCNT-COOH **1a** disappears when adenine is covalently attached to the nanotubes. For comparison, Figure 3c shows the ^{13}C resonances of 3-(6-amino-9*H*-purin-9-yl)propanoic acid **4** alone.

Exploiting the base-pairing properties of the nucleobases for the development of novel electrochemical biosensors for the recognition of complementary nucleobases or specific nucleic acid sequences,[33] a preliminary study of the electrical properties of the nucleobase−CNT hydrids in solution was performed. This is a prerequisite to determine the optimum electrochemical conditions in view of the future attachment of these CNT hybrids to semiconducting and metallic electrode surfaces. The cyclic voltammograms of *f*-SWCNT **2a** and **2b** in the 1:1 MeOH/H_2O solvent mixture containing $LiClO_4$ at 0.2 M as the supporting electrolyte are shown in Figure 4A, together with the cyclic voltammetry (CV) of acid-substituted SWCNT-COOH **1a**. Under these electrolytic conditions, none of these CNT samples showed a reduction wave. Upon oxidation, a single irreversible anodic shoulder was observed only in the CV of **2a** at a potential above 1.2 V vs SCE, i.e., at the beginning of the background electrolyte discharge. In contrast, both **2b** and **1a** showed no significant anodic step. In order to obtain a better-resolved electrochemical response, differential pulse voltammetry (DPV) was also used. The DPV of **2a** evidenced clearly a single anodic

(30) Bac, C. G.; Bernier, P.; Latil, S.; Jourdain, V.; Rubio, A.; Jhang, S. H.; Lee, S. W.; Park, Y. W.; Holzinger, M.; Hirsch, A. *Curr. Appl. Phsy.* **2001**, *1*, 149–155.
(31) Cahill, L. S.; Yao, Z.; Adronov, A.; Penner, J.; Moonoosawmy, K. R.; Kruse, P.; Goward, G. R. *J. Phys. Chem. B* **2004**, *108*, 11412–11418.
(32) Engtrakul, C.; Davis, M. F.; Gennett, T.; Dillon, A. C.; Jones, K. M.; Heben, M. J. *J. Am. Chem. Soc.* **2005**, *127*, 17548–17555.
(33) Opdahl, A.; Petrovykh, D. Y.; Kimura-Suda, H.; Tarlov, M. J.; Whitman, L. J. *Proc. Natl. Acad. Sci. U.S.A.* **2007**, *104*, 9–14.

system at 1.25 V, while weakly intense peaks at 0.13 and 0.77 V and an ill-defined broad shoulder at ca. 1.3 V were present in the DPV of **2b** (Figure 4B). The DPV of **1a** also confirmed that these SWCNTs showed no redox activity upon oxidation. The system observed at 1.25 and 1.3 V in the DPV of **2a** and **2b**, respectively, can be ascribed to the multielectronic oxidation of the bound adenine moieties.[34,35] The observation of a more intense peak for **2a** with respect to **2b** is intriguing and could be caused by the higher density of bound adenine (as proved by TGA) and the shorter distance between the CNTs, enabling faster electronic communication with the electrode surface. The occurrence of small peaks at 0.13 and 0.77 V in the DPV of **2b** was unclear and could be attributed to the presence of small redox-active impurities adsorbed on the SWCNTs.

Structural Organization and Complexation Studies of Nucleobase−Carbon Nanotube Hybrids. New developments in the production of well-controlled aligned CNT arrays pave the way for finding applications in bioelectronics and nanobiotechnology, including electrochemical enzyme-based biosensors, immunosensors, and DNA sensors.[36] Well-aligned CNTs have been synthesized mostly by chemical vapor deposition approaches,[37] under ultrahigh vacuum,[38] or utilizing very dense growth which forces the tubes to align parallel to each other.[39] Both vertically and horizontally aligned CNTs can be used in field electron emission devices.[40,41] It has also been demonstrated that incorporation of aligned CNTs in the adhesive layer enhances the through-thickness thermal conductivity in the adhesively bonded joints.[42] The production of well-aligned carbon nanostructures involves harsh conditions, and there are additional limitations for vertically aligned CNTs due to the presence of metal at the tip.[37−39,43−45] In our case, we were able to observe the horizontal alignment of CNT functionalized with adenine using atomic force microscopy (AFM).

The adenine−CNT hybrids were observed directly by transmission electron microscopy (TEM) and AFM. The TEM images of adenine-based *f*-SWCNT **2a** and **2b** are shown in Figure 5. Figure 5a displays bundles of *f*-SWCNT **2a** deposited from a methanol−H_2O (1:1) solution onto a carbon-coated TEM grid. Nanotube bundles such as those shown in Figure 5a were observed throughout. It cannot be appraised whether these bundles were present in solution or were subsequently formed,

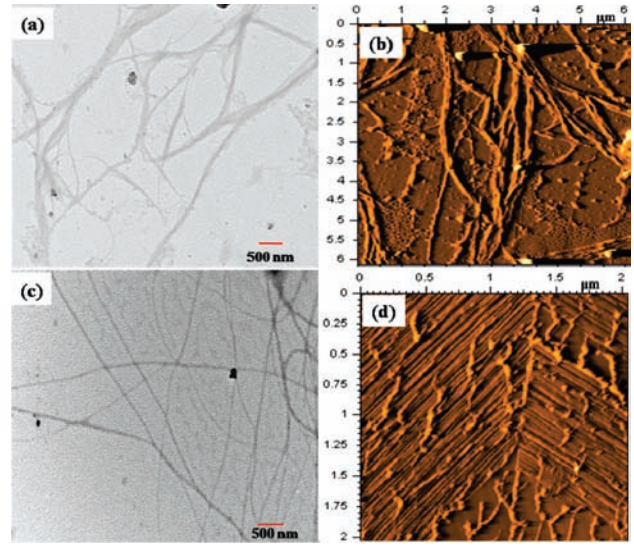

Figure 5. TEM and AFM micrographs images of adenine−CNT hybrids. (a) TEM image of *f*-SWCNT **2a** showing the bundles of nanotubes. (b) AFM images of *f*-SWCNT **2a** taken on HOPG surface. (c) TEM image of *f*-SWCNT **2b** showing exfoliation of nanotubes. (d) AFM images of *f*-SWCNT **2b** taken on HOPG surface showing alignment of the nanotubes.

due to the decrease of solubility during the slow solvent evaporation of the TEM deposition process. However, in comparison to oxidized SWCNT **1a** (Figure SI-1, Supporting Information), the bundles are more dissociated and less tightly bound with each other, which further confirmed the functionalization with adenine and its role in modulating the dispersibility properties of CNTs. The TEM images of *f*-SWCNT **2b**, which was mostly exfoliated and well dispersed, forming very small bundles (Figure 5c), are more interesting in comparison to those of *f*-SWCNT **2a** and oxidized SWCNTs. As can be seen from the images, tubes remained largely intact after functionalization. The presence of small bundles of nanotubes for *f*-SWCNT **2b** in the TEM might be due to the presence of the triethylene glycol (TEG) linker, which helps in intercalating the large bundles to produce smaller aggregate (see Supporting Information, Figures SI-2 and 3).

AFM images of adenine−CNT hybrids taken on HOPG surfaces further confirmed covalent modification and revealed fine structures of nanotubes. From comparison of the AFM images of SWNT-COOH **1a** (Supporting Information, Figure SI-4), *f*-SWCNT **2a**, and *f*-SWCNT **2b** (Figure 5), obtained by depositing the samples using the same procedure and solvent, we observed that nanotubes are still present in bundles; however, the average thickness of the bundles is much reduced after functionalization, which was confirmed by evaluating the height and diameter profile of nanotubes.

AFM images of *f*-SWCNT **2a** in methanol−H_2O (1:1) show that carbon nanotubes associated together to form thick bundles randomly placed all over the HOPG surface (Figure 5b), with a width of approximately 40−60 nm and height between 5 and 10 nm. AFM images of *f*-SWCNT **2b** deposited on HOPG display the very interesting feature of horizontally aligned nanotubes along the surface. Some tubes aligned in the center, and most of the tubes seemed to radiate from the center, giving a "leaf" or "feather" morphology (Figure 5d). This morphology has been reproducibly observed all over the surface in a series of repeated experiments. From the cross-sectional height and diameter analysis of the AFM images of *f*-SWCNT **2b** (Figure

(34) Dryhurst, G.; Elving, P. J. *J. Electrochem. Soc.* **1968**, *115*, 1014–1020.
(35) (a) Oliveira-Brett, A. M.; Antonio da Silva, L.; Brett, C. M. A. *Langmuir* **2002**, *18*, 2326–2330. (b) Zhang, X.; Jiao, K.; Liu, S.; Hu, Y. *Anal. Chem.* **2009**, *81*, 6006–6012.
(36) Katz, E.; Willner, I. *ChemPhysChem* **2004**, *5*, 1084–1104.
(37) Dai, H. *Acc. Chem. Res.* **2002**, *35*, 1035–1044.
(38) Hovel, H.; Bodecker, M.; Grimm, B.; Rettig, C. *J. Appl. Phys.* **2002**, *92*, 771–777.
(39) Choi, G. S.; Cho, Y. S.; Hong, S. Y.; Park, J. B.; Son, K. H.; Kim, D. J. *J. Appl. Phys.* **2002**, *91*, 3847–3854.
(40) (a) Srivastava, S. K.; Vankar, V. D.; Sridhar Rao, D. V.; Kumar, V. *Thin Solid Films* **2006**, *515*, 1851–1856. (b) Cao, A.; Ci, L.; Li, D.; Wei, B.; Xu, C.; Liang, J.; Wu, D. *Chem. Phys. Lett.* **2001**, *335*, 150–154.
(41) (a) Jung, S. M.; Jung, H. Y.; Suh, J. S. *Carbon* **2008**, *46*, 1973–1977. (b) Jung, S. M.; Jung, H. Y.; Suh, J. S. *Carbon* **2007**, *45*, 2917–2921. (c) Jung, S. M.; Hahn, J.; Jung, H. Y.; Suh, J. S. *Nano Lett.* **2006**, *6*, 1569–1573.
(42) Sihn, S.; Ganguli, S.; Roy, A. K.; Qu, L.; Dai, L. *Compos. Sci. Technol.* **2008**, *68*, 658–665.
(43) Yang, Q.; Chen, W.; Xiao, C.; Hirose, A.; Sammynaiken, R. *Diamond Relat. Mater.* **2005**, *14*, 1683–1687.
(44) Hubler, U.; Jess, P.; Lang, H. P.; Guntherodt, H. J.; Salvetat, J. P.; Forro, L. *Carbon* **1998**, *36*, 697–700.
(45) Kusunoki, M.; Suzuki, T.; Hirayama, T.; Shibata, N. *Physica B* **2002**, *323*, 296–298.

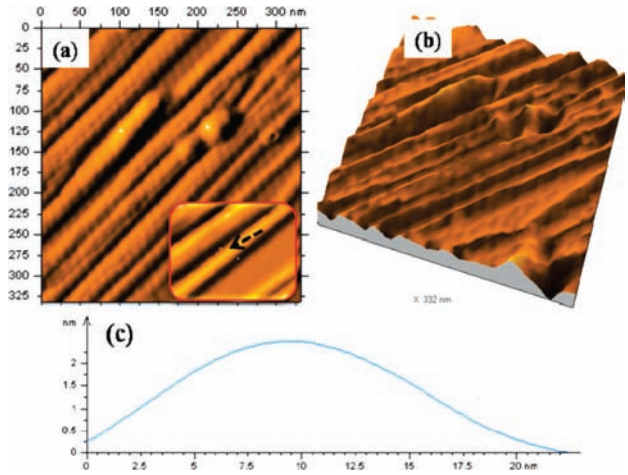

Figure 6. AFM images *f*-SWCNT **2b** on HOPG surface, showing alignment of the nanotubes. (a) AFM image of *f*-SWCNT **2b**. Inset: zoomed region. (b) 3D AFM image of *f*-SWCNT **2b** showing the heights of the nanotubes on the surface. (c) Diameter−height profile corresponding to one bundle of *f*-SWCNT **2b**, indicated by the arrow in the panel (a) inset.

6), we observed that some of the evaluated objects show height less than 2.5 nm and width below 20 nm. These dimensions are likely due to there being few parallel SWCNTs. However, the majority of the objects show cross-sectional height between 2 and 8 nm and width between 20 and 40 nm (see also Supporting Information, Figures SI-5 and 6), indicating the formation of small, regular, and homogeneous bundles.

The AFM images of SWCNT-COOH **1a** on HOPG surface shows average diameter around 60−120 nm, with height varying from 40 to 60 nm (Supporting Information, Figure SI-4), with globular and unresolved fine structures. Similarly, AFM images of *f*-SWCNT **1b** showed heavy bundles of nanotubes (Supporting Information, Figure SI-7). For comparison, we have taken the AFM images of *f*-SWCNT **2a** and *f*-SWCNT **2b** on a mica surface, showing unresolved clusters.

The binding of SWCNT on a graphite surface is similar to the interaction of two graphite planes, involving weak van der Waals interaction. It has been reported that special alignment of the lattice of the SWCNT grown on the HOPG surfaces maximizes the interaction energy.[46] It is also known that interaction between surface−adsorbate and adsorbate−adsorbate involving nucleobases is critical in creating ordered surface assemblies.[47,48] Nucleobases can exhibit formation of organized assemblies via hydrogen-bonding interactions.[49−51] It is clear that the formation mechanism of such assemblies, particularly in aqueous environments, involves adsorption followed by rearrangement of molecules on the surface into hierarchial assemblies.[52,53] The parallel-oriented surface assemblies for *f*-SWCNT **2b** can be attributed to the presence of TEG monomethyl ether chains (Figure 6). Observing force microscopy data, we believe that, subsequent to the adsorption of SWCNTs on HOPG surface, interdigitation of TEG chains at the tips and side walls of *f*-SWCNT **2b** occurs in order to keep the nanotubes apart, while adenine moieties present at the end of the TEG chains undergo self-hydrogen-bonding interactions.[51a] A similar phenomenon at the end of the SWCNT walls would explain elongation of the nanotubes to several micrometers. In contrast, when SWCNT **2a**, devoid of TEG chains, was deposited, fibrils of tubes were observed (Figure 5b). These aggregates may emerge due to van der Waals interaction between the nanotubes, which form in this case nonordered structures. From TEM experiments, it is also clear that *f*-SWCNT **2b** shows more exfoliation of nanotubes in comparison to **2a**, thus supporting our assumption. If we consider the solution behavior of such hybrids, the chances of intermolecular hydrogen bonding, via adenine−adenine base-pairing, in protic solvents (water−methanol) will be very low. As a consequence, hydrogen-bonding and hydrophobic interactions likely play crucial roles in the assembly process at the HOPG surface.[52,53]

Having in hand these nucleobase−nanotube hybrids, we finally decided to analyze the possibility of complexation with metal ions. Carbon nanotube functionalization with metal ions or metal nanoparticles is expected to further broaden their materials applications. As a consequence, several avenues are pursued for the decoration of CNT surfaces with metal ions. One approach involves covalent attachment of known coordinating ligands such as terpyridine to the surface of CNTs, where suitable metal ions may yield modified CNT architectures with tunable chemical, physical, electronic, and optical properties based on the metal ions used.[54] In another approach, oxidized nanotubes were directly interacted with silver and nickel salts through an electroless deposition method, followed by reduction with the help of ascorbic acid.[55] Recently, silver nanoparticle-decorated CNTs were prepared using silver acetate as the thermal decomposable precursor without the use of any reducing agent or electric current.[56]

We decided to exploit the coordination behavior of adenine nucleobase, attached to the CNT surface, to generate Ag(I) nanoparticle−CNT conjugates. This approach was expected to coalesce nanotubes, as it is possible to envisage recruitment of multiple CNTs via adenine units attached to their surface. Nucleic acids can coordinate to metal ions through the participation of the base keto-oxygen atoms, the heterocyclic ring nitrogen atoms, the sugar hydroxyl groups, and the phosphate

(46) Rettig, C.; Bodecker, M.; Hovel, H. *J. Phys. D Appl. Phys.* **2003**, *36*, 818–822.
(47) Li, S.-S.; Yan, H.-J.; Wan, L.-J.; Yang, H.-B.; Northrop, B. H.; Stang, P. J. *J. Am. Chem. Soc.* **2007**, *129*, 9268–9269.
(48) (a) Badin, M. G.; Bashir, A.; Krakert, S.; Strunskus, T.; Terfort, A.; Wö ll, C. *Angew. Chem., Int. Ed.* **2007**, *46*, 3762–3764. (c) Barth, J. V.; Costantini, G.; Kern, K. *Nature* **2005**, *437*, 671–679.
(49) Sivakova, S.; Rowan, S. J. *Chem. Soc. Rev.* **2005**, *34*, 9–21.
(50) (a) Jatsch, A.; Kopyshev, A.; Mena-Osteritz, E.; Bauerle, P. *Org. Lett.* **2008**, *10*, 961–964. (b) Piana, S.; Bilic, A. *J. Phys. Chem. B* **2006**, *110*, 23467–23471. (c) Heckl, W. M.; Smith, D. P.; Binnig, G.; Klagges, H.; Hansch, T. W.; Maddocks, J. *Proc. Natl. Acad. Sci. U.S.A.* **1991**, *88*, 8003–8005. (d) Xu, S.; Dong, M.; Rauls, E.; Otero, R.; Linderoth, T. R.; Besenbacher, F. *Nano Lett.* **2006**, *6*, 1434–1438.
(51) (a) Fathalla, M.; Lawrence, C. M.; Zhang, N.; Sessler, J. L.; Jayawickramarajah, J. *Chem. Soc. Rev.* **2009**, *38*, 1608–1620. (b) Xu, W.; Kelly, R. E. A.; Otero, R.; Schock, M.; Loegsgaard, E.; Stensgaard, I.; Kantorovich, L. N.; Besenbacher, F. *Small* **2007**, *3*, 2011–2014. (c) Mamdouh, W.; Kelly, R. E. A.; Dong, M.; Kantorovich, L. N.; Besenbacher, F. *J. Am. Chem. Soc.* **2008**, *130*, 695–702. (d) Gottarelli, G.; Masiero, S.; Mezzina, E.; Pieraccini, S.; Rabe, J. P. *Chem.−Eur. J.* **2000**, *6*, 3242–3248. (e) Kelly, R. E. A.; Kantorovich, L. N. *J. Mater. Chem.* **2006**, *16*, 1894–1905.
(52) Kumar, A. M. S.; Fox, J. D.; Buerkle, L. E.; Marchant, R. E.; Rowan, S. J. *Langmuir* **2009**, *25*, 653–656.
(53) (a) Kumar, A. M. S.; Sivakova, S.; Fox, J. D.; Green, J. E.; Marchant, R. E.; Rowan, S. J. *J. Am. Chem. Soc.* **2008**, *130*, 1466–1476. (b) Bestel, I.; Campins, N.; Marchenkoc, A.; Fichouc, D.; Grinstaffd, M. W.; Barthélémy, P. *J. Colloid Interface Sci.* **2008**, *323*, 435–440.
(54) Hwang, S.-H.; Moorefield, C. N.; Dai, L.; Newkome, G. R. *Chem. Mater.* **2006**, *18*, 4019–4024.
(55) Jin, G.-P.; Baron, R.; Rees, N. V.; Xiao, L.; Compton, R. G. *New J. Chem.* **2009**, *33*, 107–111.
(56) Lin, Y.; Watson, K. A.; Fallbach, M. J.; Ghose, S.; Smith, J. G., Jr.; Delozier, D. M.; Cao, W.; Crooks, R. E.; Conell, J. W. *ACS Nano* **2009**, *3*, 871–884.

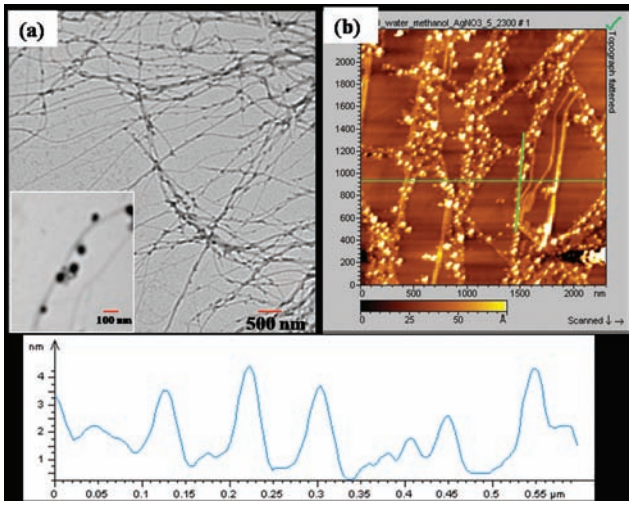

Figure 7. TEM and AFM micrograph images of *f*-SWCNT **2a** with Ag(I). (a) TEM image showing interaction of *f*-SWCNT **2a** with Ag(I). Inset: magnified TEM image showing the attachment of Ag(I) nanoparticle on nanotube. (b) AFM image of *f*-SWCNT **2a** on HOPG showing the attachment of Ag(I) nanoparticles all over the nanotube network. (c) Height and diameter profile of the AFM image in panel (b) along the green vertical line.

oxygen atoms.[57] In this vein, we have already described silver−adenine complexes that afford metallaquartets and other metal-mediated polyads.[58] We had also reported the use of polymerizable adenine nucleobases to create catalytic polymers where the activity profiles are dictated by judicious selection of impregnated metal ions.[59] Similarly, we have invoked the metal-ion coordination ability of adenine for the complexation of *f*-SWCNT **2a** with Ag(I) ions and observed the interaction with microscopy techniques. We chose *f*-SWCNT **2a** derivative for complexation with Ag(I) because *f*-SWCNT **2b** contains the additional TEG linker, which possesses the ability to bind with Ag(I) because of the presence of O and N atoms.[58] In the TEM image of *f*-SWCNT **2a** complexed with Ag(I), we observed beadlike Ag(I) nanoparticles present over the nanotubes, probably due to the interaction of adenine with Ag(I) ion (Figure 7a). In the AFM images, we saw the same interaction, with the Ag(I) nanoparticles following a path of CNT network (Figure 7b). The height and diameter profile analysis (Figure 7c) showed that the height of the nanotube varies from 4 to 6 nm, whereas the approximate height of the Ag(I) nanoparticle ranges between 3.5 and 4 nm, with an approximate width of 40−60 nm (Figure 7c and Supporting Information, Figure SI-8).

The possibility that the presence of these nanoparticles on nanotubes results from the aggregation of nanotubes themselves in the sample could be ruled out, first because the approximate dimension of the nanoparticles is around 4 nm, as observed using AFM, and second because the nanoparticles are present only on the nanotube and not on the free surface used for imaging. We also observed bigger clusters of Ag(I) metal itself, but these clusters were present only on the nanotube (Supporting Information, Figure SI-9). As a control experiment, we mixed the $AgNO_3$ solution with SWCNT-COOH **1a** and observed the sample by TEM. TEM images showed only physical adsorption of heavy clusters of Ag(I) on the surface as well as on the bundles of nanotubes, and these Ag(I) particles are not aligned (Supporting Information, Figure SI-10), thus confirming the adenine-Ag(I) interactions.

Conclusion

In summary, we have described the synthesis of new hybrids based on adenine−carbon nanotubes following the oxidation of single-walled carbon nanotubes and subsequent amidation reaction. The conjugates have been fully characterized using complementary analytical techniques. The functionalization imparted interesting features to the functionalized nanotubes. Indeed, the adenine−CNTs were able to form horizontally aligned structures reminiscent of "leaf" or "feather" morphology on HOPG surface. Such ordered organization is likely induced by the presence of the nucleobases and the TEG chains, which eventually interdigitate, allowing exfoliation and parallel arrangement. The capacity of nanotubes to self-assemble and easily align has potential applications in the development of advanced electronic nanodevices. In addition, the demonstrated capacity of the adenine−CNTs to coordinate metal ions can be exploited for novel biosensors and in heterogeneous catalysis. Work is in progress in our laboratories along these lines.

Experimental Section

Materials and Methods. HiPco nanotubes were purchased from Carbon Nanotechnologies Inc. (lot R0496). Adenine derivatives **3** and **4** were synthesized according to slightly modified literature procedures and characterized spectroscopically.[60] Reagents and solvents were purchased from Fluka, Aldrich, Loba Chemie Pvt. Ltd. (Mumbai, India), Spectrochem (Mumbai, India). and S.D. Finechem Ltd. (Mumbai, India) and used without further purification unless otherwise stated. Moisture-sensitive reactions were performed under argon or N_2 atmosphere. CH_2Cl_2 was freshly distilled from CaH_2 and THF from Na/benzophenone, and DMF was dried over 4 Å molecular sieves. Chromatographic purification was done with Merck silica gel (Kiesegel 60, 40−60 μm, 230−400 mesh ASTM) in a standard column. TLC was performed on aluminum sheets coated with silica gel 60 F254 (Merck, Darmstadt). ^{1}H and ^{13}C NMR spectra were recorded on JEOL-JNM LAMBDA 400 (operating at 400 and 100 MHz, respectively), JEOL ECX-500 (operating at 500 and 125 MHz, respectively), and Bruker DPX 300 instruments. The peak values were obtained as ppm (δ) and referenced to the solvent.

Preparation of SWCNT-COOH 1a. In 150 mL of 3 M HNO_3, 200 mg of pristine HiPco SWCNTs were suspended by sonication. The mixture was refluxed for about 48 h, sonicated for 1 h, and refluxed for another 48 h. Then, 50 mL of 3 M HNO_3 was added, and after sonication for 2 h, the mixture was again refluxed for 12 h. The resultant suspension was then diluted by deionized water, filtered through a polycarbonate filter (Isopore, pore size 100 nm), and rinsed thoroughly with deionized water several times until the pH was ~7. The resulting SWCNTs were resuspended in deionized water and sonicated for 5 min. The suspension was then again filtered. The black product obtained was dried and characterized by TEM (Figure SI-1), AFM, and TGA.

Preparation of *f*-SWCNT 1b. A suspension of 20 mg of oxidized SWCNT-COOH **1a** in 8 mL of oxalyl chloride was stirred at 62 °C for 24 h under an Ar atmosphere. The excess of oxalyl chloride was evaporated under a vacuum, giving SWCNT-COCl.

(57) Saenger, W. *Principles of Nucleic Acid Structure*; Springer: New York, 1984.
(58) (a) Purohit, C. S.; Mishra, A. K.; Verma, S. *Inorg. Chem.* **2007**, *46*, 8493–8495. (b) Purohit, C. S.; Verma, S. *J. Am. Chem. Soc.* **2007**, *129*, 3488–3489. (c) Purohit, C. S.; Verma, S. *J. Am. Chem. Soc.* **2006**, *128*, 400–401.
(59) Srivatsan, S. G.; Parvez, M.; Verma, S. *Chem.−Eur. J.* **2002**, *8*, 5184–5191.
(60) (a) Soulere, L.; Sturm, J. C.; Nunez-Vergara, L. J.; Hoffmann, P.; Perie, J. *Tetrahedron* **2001**, *57*, 7173–7181. (b) Weisser, M.; Kashammer, J.; Menges, B.; Matsumoto, J.; Nakamura, F.; Ijiro, K.; et al. *J. Am. Chem. Soc.* **2000**, *122*, 87–95.

A mixture of 10 mg of SWCNT-COCl and 120 mg of Boc-$NH(CH_2CH_2O)_2$-$CH_2CH_2NH_2$ in 10 mL of dry THF was heated at reflux for 48 h. After cooling to room temperature, solvent was evaporated under a vacuum. The black suspension of methanol was suspended in diethyl ether to remove excess protected amine. The black precipitate separated out after some time, and then the suspension was centrifuged. The resulting Boc-protected SWCNTs were dried at room temperature under a vacuum. A 7 mg portion of Boc-protected SWCNTs was suspended in 3 mL of 4 M HCl in dioxane and stirred at room temperature for 12 h under an Ar atmosphere to cleave the Boc group at the chain-end. The solvent was evaporated. *f*-SWCNT **1b** was washed with dichloromethane and methanol several times and finally with diethyl ether and the dried under a vacuum. The amount of functional groups per gram of *f*-SWCNT **1b** (loading) was measured with the quantitative Kaiser test (0.6 mmol/g). The nanotubes were characterized by TEM, AFM, and TGA.

Preparation of *f*-SWCNT 2a. Fifteen milligrams of SWCNT-COCl was suspended in a solution of **3** (62 mg, 150 μmol) and diisopropylethylamine (DIEA) (80 μL, 460 μmol) in 15 mL of dry THF. The resulting suspension was heated under reflux for 48 h. After cooling to room temperature and removing the excess of **3** by washing several times with DMF, methanol, and finally diethyl ether, the product was dried at room temperature under a vacuum to afford 13.5 mg of *f*-SWCNT **2a**. The nanotubes were characterized by TEM, AFM, and TGA.

Preparation of *f*-SWCNT 2b. SWCNT-TEG-$NH_3^+Cl^-$ **1b** (14 mg, 8.4 μmol, based on the loading calculated with the quantitative Kaiser test) was dissolved in 2 mL of DMF and neutralized with DIEA (7.3 μL, 8.39 μmol). A solution of compound **4** (35 mg, 169 μmol) in 2 mL of a mixture of DCM−DMF (1:1) was activated with 1-ethyl-3-(3-dimethylaminopropyl)carbodiimide hydrochloride (EDC × HCl) (48.61 mg, 251 μmol) and *N*-hydroxybenzotriazole (HOBt) (34.2 mg, 251 μmol) for 1 h under argon and subsequently added to the carbon nanotube solution. The resulting mixture was stirred for 24 h at room temperature, and the reaction mixture was then filtered on a polycarbonate filter (Fluoropore, pore size 100 nm). The black solid collected on the filter was redissolved in DMSO and filtered again. This procedure was repeated two times each with DMSO and CH_2Cl_2−MeOH (10:1) mixture to remove the excess of **4**. After the final washings with diethyl ether, the black solid was dried under a vacuum to afford 12.5 mg of *f*-SWCNT **2b**. The nanotubes were characterized by TEM, AFM, and TGA.

Preparation of Ag(I) Complex of *f*-SWCNT 2a. In 0.1 mL of 1:1 methanol−water, 0.1 mg of the *f*-SWCNT **2a** and SWCNT-COOH **1a** (used as control) were dispersed by ultrasonication for 5 min. Similarly, a solution of $AgNO_3$ was prepared. The $AgNO_3$ solution was added to **2a** and **1a**. The solution of **2a** or **1a** was shaken thoroughly, ultrasonicated for 5 min, and then kept aside for 10−12 h. Ten microliters of the solution of **2a** or **1a** was deposited onto a holey-carbon TEM grid and HOPG surface and dried. The adenine-modified nanotube−Ag(I) complexes were characterized by TEM and AFM.

Characterization. Thermogravimetric analyses (TGA) were performed using a TA Instruments TGA Q500 with a ramp of 10 °C/min under N_2 from 100 to 900 °C. FT-IR analysis was carried out on Perkin-Elmer SpectrumOne instrument using the potassium bromide (KBr) pellet method. About 1 mg of nanotubes was mixed and ground with specially dried KBr (∼100 mg), and then the powder was compressed in a special metal die under pressure to produce transparent KBr discs. Transmission electron microscopy (TEM) was performed on a Hitachi H600 microscope and a Philips 208 microscopy, working at different accelerating voltage and different magnification. A 0.1 μg portion of the sample was dispersed in 0.1 mL of methanol−water (1:1) by ultrasonication for 5 min and kept for 10−12 h. The solution was again ultrasonicated for 5 min before 10 μL was deposited onto a holey-carbon TEM grid and dried. The images are typical and representative of the samples under observation. Atomic force microscopy (AFM) was carried out using an Agilent Technologies atomic force microscope (Model 5500) operating in noncontact/ACAFM mode. Micro-fabricated silicon nitride cantilevers with a spring constant (*C*) of ∼50 N/m and resonant frequency (*f*) of 175 kHz were used. The average thickness (*T*), width (*W*), and length (*L*) of the cantilever were approximately 700, 38, and 225 μm, respectively. Data acquisition and analysis was carried out using PicoView 1.4 and Pico Image Basic software, respectively. For AFM imaging, 0.1 μg portions of the samples were dispersed in 0.1 mL of methanol−water (1:1) by ultrasonication for 5 min and kept for 10−12 h. The solution was again ultrasonicated for 5 min before depositing, and 10 μL was deposited onto a HOPG surface and dried under lamp for 15 min followed by drying under a vacuum for 2 h. Solid-state nuclear magnetic resonance experiments were conducted on an AVANCE 500 MHz wide-bore spectrometer (Bruker, Wissembourg, France) operating at a frequency of 125.7 MHz for ^{13}C and equipped with a triple-resonance MAS probe designed for 3.2 mm zirconia rotors (closed with Kel-F caps). All the samples were spun at 15 kHz spinning frequency. All cross-polarization $^1H/^{13}C$ experiments were carried out with a proton pulse of 3.12 μs, a spin-lock field of 80 kHz for proton and 60 kHz for carbon, a decoupling field of 100 kHz, a 1.2 ms contact time, and a recycle time of 5 s. Owing to the spectral line widths and in order to get undistorted lineshapes, we also made use of Hahn's echo pulse sequence[61] synchronized with the rotation (echo time = *n* rotation periods). The total echo time was kept identical in all spectra and equal to two rotation periods (τ = 66.7 μs). Linear potential sweep cyclic voltammetry (CV) and differential pulse voltammetry (DPV) experiments were performed with an Autolab PGSTAT 20 potentiostat from Eco Chemie B.V., equipped with General Purpose Electrochemical System (GPES) software. A methanol (VWR, HPLC grade)/water (ultrapure, 18.2 MΩ cm) (1/1 v:v) mixture containing 0.2 M lithium perchlorate, $LiClO_4$ (Fluka, purum >98%, stored in a desiccator), was used as the electrolytic medium. The SWCNT samples were sonicated for at least 30 min in this electrolytic medium prior to electrochemical measurements. The working electrode was a 3-mm-diameter glassy carbon disk (area 0.07 cm^2) and was polished successively with 5 μm silicon carbide paper (Struers, FEPA P no. 4000) and 0.25 μm alumina slurry (Struers). The counter electrode was a glassy carbon rod. Potentials were relative to a platinum wire and were calibrated vs saturated calomel electrode (SCE) by adding ferrocenemethanol at the end of the experiments. In the used electrolytic medium, the ferrocenemethanol/ferroceniummethanol couple was observed at $E^{\circ\prime}$ = 0.16 V vs Pt wire. All potentials indicated in the text are referred to SCE (uncertainty ±0.01 V). Electrochemical measurements were carried out at room temperature (20 ± 2 °C) and inside a homemade Faraday cage under a constant flow of argon.

Acknowledgment. This work was supported by the French-Indian CEFIPRA/IFCPAR collaborative project (Project no. 3705-2). P.S. wishes to thank CEFIPRA/IFCPAR for a postdoctoral fellowship. TEM images were recorded at the RIO Microscopy Facility Plate-form of Esplanade Campus (Strasbourg, France). AFM images were recorded on an Agilent 5500 series instrument (IIT-Kanpur, India).

Supporting Information Available: Additional characterization images. This material is available free of charge via the Internet at http://pubs.acs.org.

JA905041B

(61) Hahn, E. L. *Phys. Rev.* **1950**, *80*, 580–594.